Simulation of the Modern Arctic Climate by the NCAR CCM1*

DAVID H. BROMWICH**,† AND REN-YOW TZENG**

**Byrd Polar Research Center, The Ohio State University, Columbus, Ohio
†Atmospheric Sciences Program, The Ohio State University, Columbus, Ohio

THOMAS R. PARISH

Department of Atmospheric Science, University of Wyoming, Laramie, Wyoming

(Manuscript received 25 October 1992, in final form 14 June 1993)

ABSTRACT

The NCAR CCM1's simulation of the modern arctic climate is evaluated by comparing a five-year seasonal cycle simulation with the ECMWF global analyses. The sea level pressure (SLP), storm tracks, vertical cross section of height, 500-hPa height, total energy budget, and moisture budget are analyzed to investigate the biases in the simulated arctic climate.

The results show that the model simulates anomalously low SLP, too much storm activity, and anomalously strong baroclinicity to the west of Greenland and vice versa to the east of Greenland. This bias is mainly attributed to the model's topographic representation of Greenland. First, the broadened Greenland topography in the model distorts the path of cyclone waves over the North Atlantic Ocean. Second, the model oversimulates the ridge over Greenland, which intensifies its blocking effect and steers the cyclone waves clockwise around it and hence produces an artificial "circum-Greenland" trough. These biases are significantly alleviated when the horizontal resolution increases to T42.

Over the Arctic basin, the model simulates large amounts of low-level (stratus) clouds in winter and almost no stratus in summer, which is opposite to the observations. This bias is mainly due to the location of the simulated SLP features and the negative anomaly of storm activity, which prevent the transport of moisture into this region during summer but favor this transport in winter.

The moisture budget analysis shows that the model's net annual precipitation ($[P - E]$) between 70°N and the North Pole is 6.6 times larger than the observations and the model transports six times more moisture into this region. The bias in the advection term is attributed to the positive moisture fixer scheme and the distorted flow pattern. However, the excessive moisture transport into the Arctic basin does not solely result from the advection term. The contribution by the moisture fixer is as large as from advection. By contrast, the semi-Lagrangian transport scheme used in the CCM2 significantly improves the moisture simulation for this region; however, globally the error is as serious as for the positive moisture fixer scheme.

Finally, because the model has such serious problems in simulating the present arctic climate, its simulations of past and future climate change for this region are questionable.

1. Introduction

The National Center for Atmospheric Research's (NCAR) Community Climate Model Version 1 (CCM1) at a spatial resolution of R15 is a widely used global climate model (GCM). However, comparatively little effort has been devoted to evaluating the model's simulation of the present climate, particularly in polar regions. The polar regions not only are the major energy sinks on earth but also play an important role in global climate change. Many GCM simulations (e.g., Washington and Meehl 1989) project a large climatic response in these areas to increased greenhouse gas concentrations. Therefore, it is important to examine the model's performance for these regions.

By comparing the CCM1 simulations to the ECMWF (European Centre for Medium-Range Weather Forecasts) analyses, Randel and Williamson (1990) showed that the CCM1 has a cold bias throughout the troposphere, a poleward eddy momentum flux in the Southern Hemisphere that is too weak, and anomalously weak westerlies in high southern latitudes. In addition, they pointed out that the positive moisture fixer scheme used in the CCM1 causes a serious error over the polar regions and over continents. Tzeng et al. (1993) found that this moisture scheme is the primary factor causing a warm bias and anomalously high precipitation over Antarctica. Furthermore, Rasch and Williamson (1990) showed that this moisture scheme

* Contribution 842 of Byrd Polar Research Center, The Ohio State University.

Corresponding author address: Dr. David H. Bromwich, Byrd Polar Research Center, Ohio State University, 108 Scott Hall, 1090 Carmack Rd., Columbus, OH 43210-1002.

has a larger bias in the Northern Hemisphere than in the Southern Hemisphere, especially over high northern latitudes.

Some of the important climatic features impacting the Arctic basin are the Icelandic low, the Aleutian low, low-level stratus clouds in summer, and a strong anticyclone over the Beaufort Sea in winter. This anticyclone steers the Transpolar Drift Stream, which transports sea ice from the Arctic Ocean to the Greenland Sea. Walsh and Crane (1992) compared the arctic climate simulated by five atmospheric GCMs (including CCM1). They pointed out that many GCMs cannot simulate the last two features, but they did not provide explanations for these model problems. Here, we investigate the performance of the CCM1 over the Arctic basin by comparing the model's output to the ECMWF global analyses. Model shortcomings and possible remedies are discussed.

The North Atlantic Ocean is an important area for the global climate system. On seasonal and shorter time scales it is the main sector for atmospheric and oceanic exchanges between the Arctic basin and lower latitudes. On longer time scales, the variable thermohaline convection off Greenland produces North Atlantic Deep Water that propagates throughout the global ocean and outcrops around Antarctica (e.g., Held 1993; Stanton 1991; and Broecker et al. 1985). These air–sea interactions are also important for exchanges of heat and CO_2 with the atmosphere (Rintoul 1992). On the ice age time scale, this area was bounded to the west by the Laurentide ice sheet and the east by the Ferro–Scandinavian ice sheet. Ironically, the NCAR CCM1's simulation of the present climate is weakest for this area.

Although the state-of-the-art NCAR CCM2 is now available at NCAR for general use, understanding the performance of the CCM1 is still very important for climatic studies and CCM users. First, this understanding provides a perspective on the limitations of past climate change simulations by the CCM1. Second, with the increasing power of workstations, researchers need not solely depend on a supercomputer to do climate simulations. A workstation can now easily run the CCM1 at R15 resolution and this has become a very practical approach for study of climate change problems. Third, the CCM2-T42 still retains many biases in its simulation of arctic climate, as briefly summarized here. Therefore, the main objectives of this paper are to evaluate the capabilities and limitations of the CCM1 and to suggest reasonable remedies for the biases in its simulation of arctic climate.

2. Model and data

The model used in this study is the standard version of CCM1 at R15 (rhomboidal truncation at wavenumber 15) horizontal resolution, equivalent to a 4.5° latitude × 7.5° longitude grid. There are 12 σ levels in the vertical ($\sigma = P/Ps$) with the lower 7 levels being in the troposphere and the other 5 levels being above the tropopause. The numerical schemes and physical parameterizations are described in detail by Williamson et al. (1987). A brief summary is presented here.

The topography in the model is truncated at R15 from high-resolution spectral data. Generally, the height of mountains is about 50% of actual and their horizontal dimensions are much larger. The distorted topography has a serious effect on the simulation of arctic climate, which is discussed in detail.

The sea surface temperature (SST) and sea ice distributions are specified by climatological data and updated in the middle of each month for seasonal cycle simulations. The surface temperatures, by contrast, are calculated over land, snow, and sea ice via a surface energy budget equation. The thickness of sea ice is prescribed to be 2 m, while the snow depth and cover change with time. The seasonal cycle of the model is basically forced by the seasonal change of SST and the daily change of the solar declination angle with a fixed solar insolation (1370 W m^{-2}) at the top of the model atmosphere. No diurnal cycle is included in the model. This may affect the calculation of surface temperature and hence the stability of the surface layer, particularly during nighttime (Hansen et al. 1983), but the effect is negligible in the Arctic (Herman and Goody 1976). The diurnal cycle is included in the CCM2 (Williamson 1990).

The model produces negative values of moisture content in arid areas due to the spectral representation of the model. To suppress these aphysical negative moisture values, a positive moisture fixer scheme is used. First, the model eliminates the negative specific humidities locally by transporting moisture vertically and longitudinally from adjacent points. Second, if the moisture from these points is not enough to correct a negative value, a globally conserving correction is made after the local correction is applied at all points. Moisture is added to the points with negative values until they are zeroed out. To offset the increase in moisture by this process, all values are decreased proportionally.

The model forms clouds that interact with the radiation parameterization (Ramanathan et al. 1983). Convective clouds are formed when one or more layers undergo moist convective adjustment. The model assumes that the clouds in each layer are randomly overlapped with maximum cloud coverage of 30% in the convective column and that they have a cloud emissivity of 1. Nonconvective clouds are formed whenever stable condensation occurs. The fractional coverage of these nonconvective clouds is assumed to be 95% and their emissivity is a function of liquid water content. No clouds of any type are formed in the very thin surface layer of the model nor in the top two layers of the model.

The CCM1 history data used here are from standard CCM1 seasonal cycle simulations with the option of

interactive surface hydrology. With this option, the wetness factor for the latent heat flux over land surfaces is determined by the soil moisture rather than specified. This gives a more realistic surface hydrological cycle. However, the logical parameters used to determine the snow cover and snow precipitation in the routine "COND" are incorrectly replaced by the logical parameter for soil moisture in the standard version of the CCM1 (R. J. Oglesby 1992, personal communication). These bugs cause snowfall in the tropics and errors in the surface temperature (energy) calculations. Note that our simulations [including those discussed by Tzeng et al. (1993)] used a corrected version of the CCM1 code. The seasonal simulation was integrated for 6 model years and the last 5 years of model data were analyzed. There are two outputs per model day (0000 and 1200).

The observational data used here are the twice-daily ECMWF global analyses (1980–1989), which are saved in the NCAR data library. The horizontal resolution of ECMWF data is 2.5° latitude by 2.5° longitude. The data were interpolated to the R15 gaussian grid for comparison with the CCM1 output. The quality of these data and the changes in analyses after 1980 are documented by Trenberth and Olson (1988).

3. Results

a. Sea level pressure (SLP)

The winter mean (DJF) of the CCM1 SLP over the last 5 model years shows a similar pattern to that of the ECMWF analyses (Fig. 1). The model captures the overall pattern of the Aleutian low, the Icelandic low, the Siberian anticyclone, a ridge over the Rocky Mountains, and a ridge over northeast Greenland. The intensity and the location of each center, however, do not match the observations in detail. For instance, the observed Icelandic low has its major axis from the Labrador Sea (55°W) to the Kara Sea (65°E) and two troughs, one along the east coast of North America and the other over the west coast of Greenland. The simulated Icelandic low also contains these two troughs, but its major axis displays a circum-Greenland pattern. Moreover, the center of the simulated Icelandic low is shifted to the west side of Greenland. These features clearly indicate that the biases in this area are directly related to the model's Greenland topography. On the other hand, the center of the simulated Siberian anticyclone is shifted southward by about 10° latitude (from the Mongolian Plateau to central China) and the primary ridge over the Arctic Ocean is now along the 90°E meridian instead of over the East Siberian Sea and the Beaufort Sea. The shift of the ridge over the Arctic Ocean and the distortion of the Icelandic low directly affect the simulation of arctic climate. The impact of these biases and their causes are discussed in the following sections.

The other notable differences between the model's SLP pattern and the observed can be found in the Aleutian Islands region. The center of the simulated Aleutian low (180°) is about 5° longitude west of the observed (175°W) and its intensity is about 5 hPa deeper. Moreover, the model shows a trough over western Alaska, which is not present in the observations. These differences between the model simulation and the observations are related to the topography of the Rocky Mountains and the activity of cyclones in the model. More discussion is given in section 3b.

Furthermore, the SLP difference between the CCM1 output and the ECMWF analyses displays a wavenumber one pattern over the Arctic basin (Fig. 1c). This difference pattern is also attributed to two factors: the model's topographic representation and the model's storm tracks. The positive SLP anomaly southeast of Greenland and negative SLP anomaly west of Greenland is due to the broadened Greenland topography, which blocks the climatological path of the North Atlantic Ocean storms. The maximum positive SLP anomaly over the eastern Arctic Ocean (80°E) also results from 1) the blocking effect of the Greenland topography, which prevents the migration of cyclones into this region and 2) the spectral representation of the sea surface. Although the sea ice is specified from monthly mean climatological data, the altitude of the model's sea surface is distorted by the spectral truncation. At R15 resolution, the altitude of the sea surface in the eastern Arctic Ocean is about 160 m above mean sea level (MSL) along 90°E and about 180 m below MSL at 30°E and 120°W (Fig. 2). Because there is permanent sea ice over the "hill" area of the eastern Arctic Ocean (90°E), this creates a semipermanent surface high pressure anomaly (in both summer and winter seasons) due to surface cooling. On the other hand, the maximum negative SLP anomaly over the Beaufort Sea (130°W) is attributable to both the blocking effect of the broadened Greenland topography and the shift of the ridge westward to 90°E. By contrast, the lack of the Beaufort Sea anticyclone in the CCM1 simulations may also relate to the uniformly prescribed sea ice thickness (2 m) as indicated by Battisti et al. (1992) from their CCM2 analysis. Additional sensitivity studies are needed to verify this hypothesis.

The model can reasonably simulate the Pacific and Atlantic subtropical anticyclones during summer (JJA) (Fig. 3) in terms of the location and intensity of their centers. Nevertheless, the main axes of the ridges are not well simulated by the model, especially for the Pacific subtropical anticyclone. The main axis of the simulated Pacific anticyclone has a southeast to northwest orientation [from its center over the northeastern Pacific Ocean to the Sea of Okhotsk (50°N, 150°E)] (Fig. 3a), while the climatological orientation of this ridge is from northeast to southwest (from the center of the anticyclone to the east coast of the Philippines). The distortion of this ridge not only affects the simulation

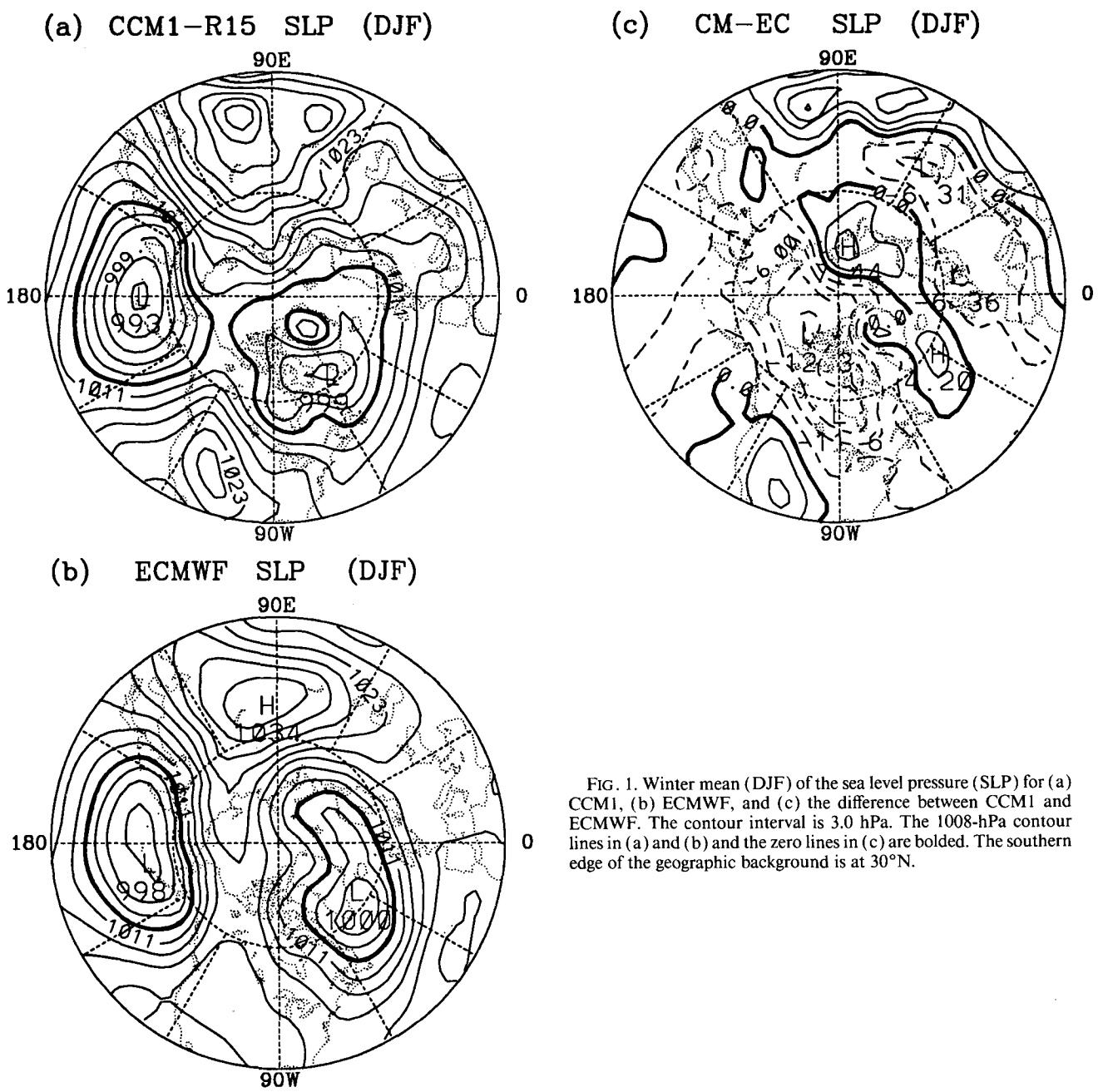

FIG. 1. Winter mean (DJF) of the sea level pressure (SLP) for (a) CCM1, (b) ECMWF, and (c) the difference between CCM1 and ECMWF. The contour interval is 3.0 hPa. The 1008-hPa contour lines in (a) and (b) and the zero lines in (c) are bolded. The southern edge of the geographic background is at 30°N.

of the Southeast Asian monsoon, but also impacts the simulation of arctic climate due to the transport of sensible heat and moisture from the tropics into the northwestern Pacific Ocean and northeastern Asia (Siberia). The distorted Pacific anticyclone may be due to the model's undersimulation of the planetary-scale waves and their misplaced phase. The impact of these waves on the arctic climate is described in the sections on 500-hPa height and energy budget analysis (sections 3d and 3e).

Figure 3c shows a positive SLP anomaly throughout the entire eastern Arctic Ocean with a maximum center around 90°E. As discussed earlier, this SLP anomaly center is due to the distorted sea surface by the spectral truncation in the model. This SLP anomaly over the Arctic basin not only affects the transport of sea ice out of the Arctic Ocean in winter but also impacts the simulation of arctic stratus clouds in summer. The model simulates almost no arctic stratus cloud (Fig. 4b) in summer but maximum stratus cloud amount in winter (Fig. 4a). This annual variation is just opposite to the observations, which show prevailing stratus clouds in summer and few low-level clouds in winter (Vowinckel and Orvig 1970). The lack of simulated

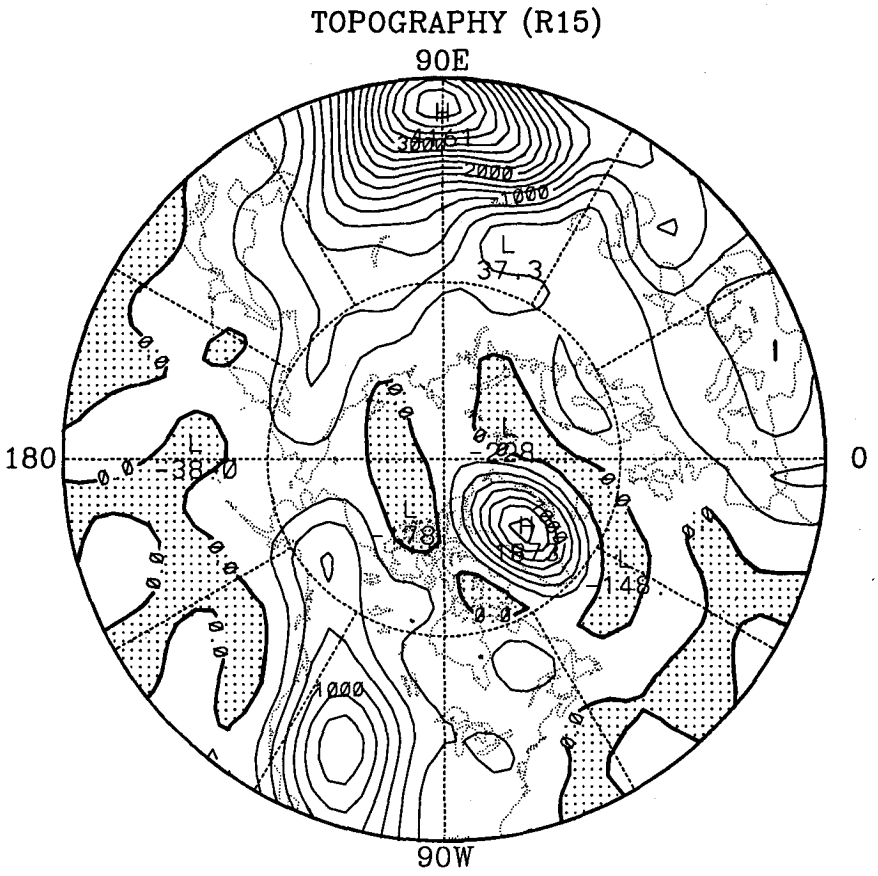

FIG. 2. The topography of the Northern Hemisphere at R15 resolution. The contour interval is 250.0 m. The zero contour lines are bolded and the negative areas are stippled.

arctic stratus clouds in summer is attributed to the location and orientation of the anticyclone over the Arctic Ocean (e.g., Tsay and Jayaweera 1984), because the arctic stratus cloud coverage is primarily maintained by the advection of warm, moist air from the surrounding landmasses into the Arctic basin (Herman and Goody 1976). The isobars of the simulated anticyclone over the Arctic basin are parallel to the coastline, which prevents the poleward transport of moisture, especially in the lower troposphere. The storm activity is also important for the transport of moisture into the Arctic basin, as discussed in the next section. In winter, the moisture supply is completely dominated by the advection because the evaporation from the frozen sea surface is very small. Therefore, the errors in the simulated wintertime low-level clouds over the Arctic basin are due to the bias in the simulated SLP, which, in turn, distorts the flow pattern over the Arctic region. In addition, the artificial positive moisture fixer scheme also has a great impact on the moisture balance. Rasch and Williamson (1990) pointed out that for this region the magnitude of the moisture fixer is 50% to 100% of the largest term (the advection term) in the moisture balance equation. More discussion of this impact is found in section 3f on the moisture budget. Finally, the absence of a proper planetary boundary-layer parameterization in the model may also contribute to the errors in the cloud simulation (e.g., Randall et al. 1985). This parameterization is included in the NCAR CCM2.

b. Storm tracks

The storm track is represented by the standard deviation of bandpass-filtered (2–6.5 day) sea level pressure. The winter (DJF) mean of the model results (Fig. 5a) shows four storm activity centers: the North Pacific Ocean, northwest Canada, the northwest Atlantic Ocean, and the northeastern Tibetan Plateau, but the ECMWF analyses exhibit only three major centers (Fig. 5b). Moreover, the intensity and pattern of the simulated storm tracks differ from those shown by the observations. The model oversimulates the storm activity over the eastern Rocky Mountains and northeastern Tibetan Plateau and the simulated storm track over the North Atlantic Ocean is not correct.

The differences between the model result and the observations are depicted in Fig. 5c. Figure 5c shows

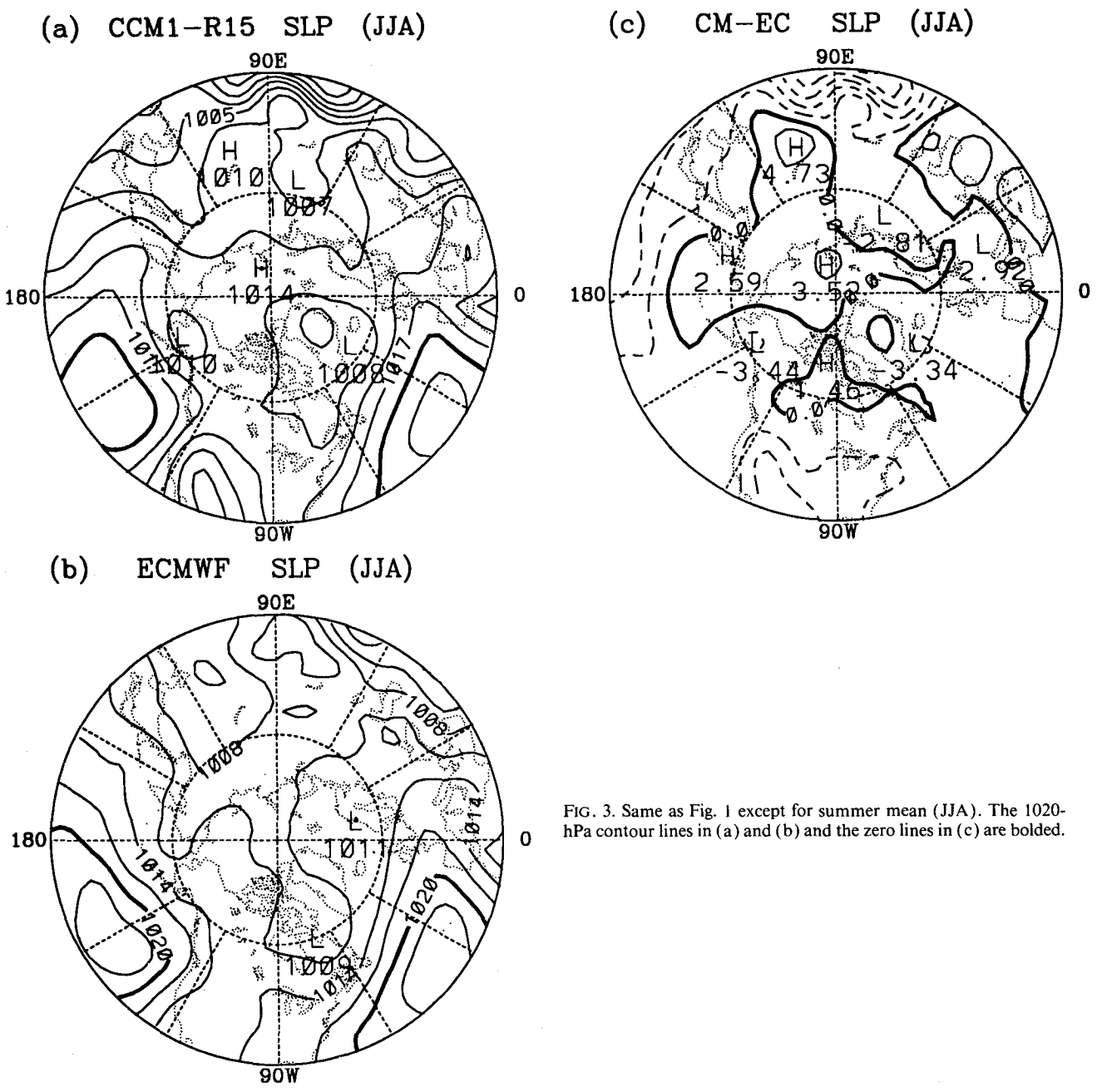

FIG. 3. Same as Fig. 1 except for summer mean (JJA). The 1020-hPa contour lines in (a) and (b) and the zero lines in (c) are bolded.

three regions with a positive anomaly of storm activity. They are the Eurasian continent along 40°N from the Mediterranean Sea to Japan, the eastern slopes of the Rocky Mountains, and west Greenland. The biases over the first two regions are on the lee side of the major mountain ranges, the Middle Asian mountains (including the Himalayas and Caucasus mountains) and the Rocky Mountains, respectively. These biases are clearly related to lee cyclogenesis. By contrast, the positive anomaly over west Greenland is attributed to the blocking effect of the broadened Greenland topography, which forces the cyclone waves to stay to the west of Greenland. Therefore, there is a maximum positive anomaly west of Greenland and a maximum negative anomaly east of Greenland. On the other hand, the positive anomalies over northwest Canada and Alaska are due to the oversimulation of the ridge over the Rocky Mountains (Fig. 1a), which intensifies the north–south exchange of energy and moisture. Moreover, the westward shift of the ridge over northeastern Siberia also favors cyclone waves moving into this region.

The model overestimates the ridge (anticyclone) over Greenland throughout the troposphere (see Fig.

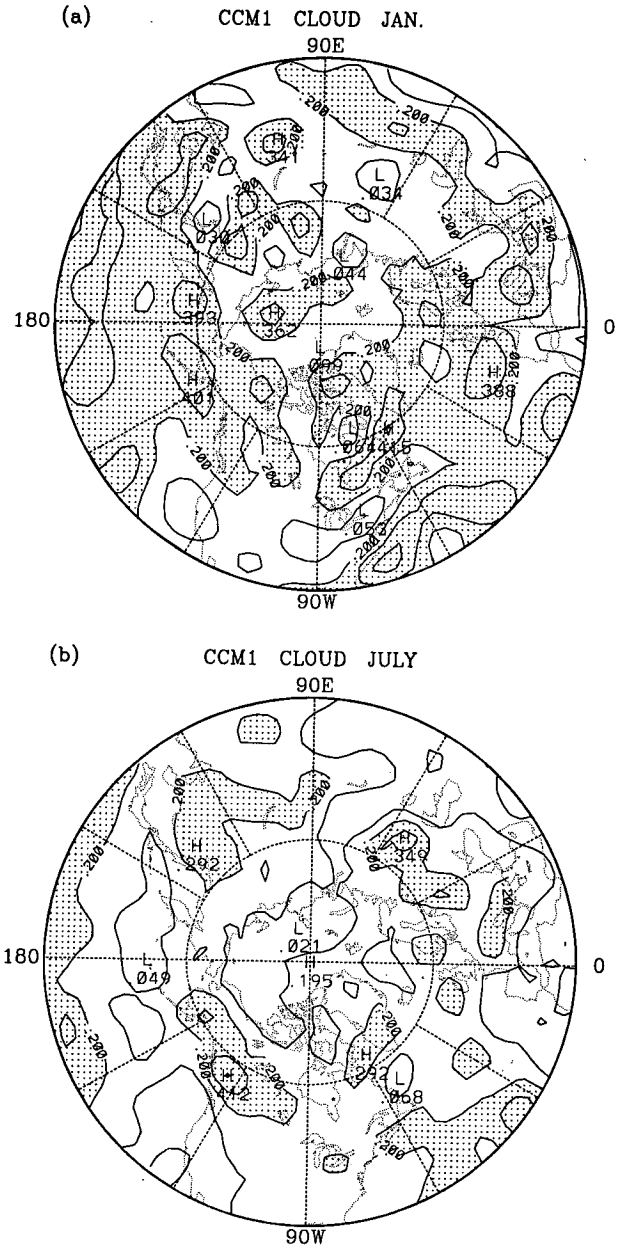

FIG. 4. The model's cloudiness in (a) January and (b) July at the second lowest sigma level (sigma = .926, about 750 m above the surface). The contour interval is 0.1. The areas greater than 0.2 are stippled.

10c, which is discussed later). This semipermanent anticyclone steers cyclone waves clockwise from the southeast coast of Greenland around the south to the west coast of Greenland. Figure 6 presents an illustrative case study of the life cycle of a simulated cyclone approaching Greenland. It shows that when the cyclone approaches Greenland, its circular shape is distorted into an oval due to the blocking effect of Greenland and the eastward movement of the cyclone wave. The distorted cyclone then breaks into two centers with the weaker one continuing across the North Atlantic Ocean to the south of Iceland, and the stronger one moving quickly along the coast of Greenland in a clockwise (anticyclonic) fashion. This stronger cyclone center starts to decay, when it migrates to the west of Greenland. After the cyclone passes northern Greenland, it slightly reintensifies over northeast Greenland. At this point, the cyclone may go in two different directions. The usual path is straight eastward from the Greenland Sea to the Norwegian Sea, and finally dissipating in the Barents Sea. However, there are some cases where the cyclone moves southward, merges with the minor cyclone center over the North Atlantic Ocean, and moves clockwise along the Greenland coast again. This process indicates that the impact of the broadened topography of Greenland can not only block the path of a cyclone but also steer it. Furthermore, these processes occur for both cyclones and anticyclones.

The summer mean of the storm activity (Fig. 7) shows that the model simulates too much storm activity in midlatitudes, especially over the continents, but it captures too little in the Arctic basin. The minimum center over the eastern Arctic basin (90°E) is due to the semipermanent high SLP over this region (Fig. 3c), which suppresses the fluctuations of weather systems in this area and blocks the cyclone waves propagating toward this region. This anticyclone and the lack of storm activity suppress the prevailing stratus clouds during summer because they both prevent the transport of moisture into this region. In addition, the positive SLP anomaly over central Canada (Fig. 3c) pushes the North American storm track southward by about 10° latitude. The model's storm track is along 45°N, but the observed storm track is along 55°N. The southward shift of the North American storm track and the positive anomaly of the storm activity over eastern Asia (Fig. 7), however, are related to the simulated planetary-scale waves, which are discussed in section 3d on the 500-hPa height. In addition, the bias of storm activity in the model is related to the positive moisture fixer scheme. Rasch and Williamson (1990) showed that the maximum error due to the artificial positive moisture fixer scheme is over these two regions (Fig. 8) in the lower troposphere. Also, they indicated that the impact of the moisture fixer in these regions is nearly as large as the largest term in the moisture balance equation and larger than any other term.

Figure 9 presents the differences in the time evolution of the storm activity between the model and observations at 45° and 70°N. At 70°N, the model oversimulates the storm activity west of Greenland (40°W) and undersimulates the storm activity east of Greenland (Fig. 9a). This indicates that the blocking effect of the broadened Greenland topography has a broadscale impact on the cyclone simulation. Moreover the model cannot simulate the semiannual variation of storm activity, which is sig-

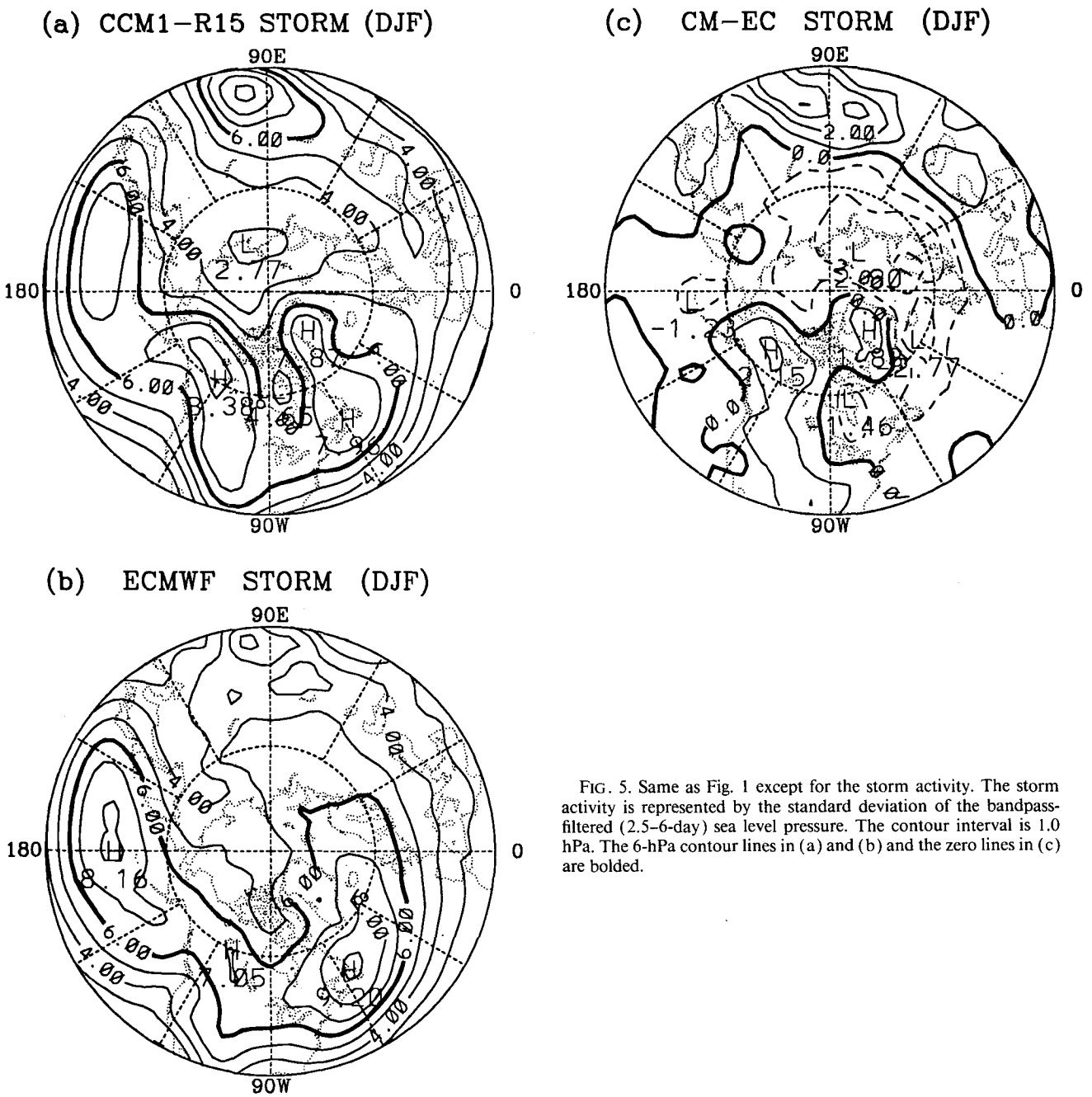

FIG. 5. Same as Fig. 1 except for the storm activity. The storm activity is represented by the standard deviation of the bandpass-filtered (2.5–6-day) sea level pressure. The contour interval is 1.0 hPa. The 6-hPa contour lines in (a) and (b) and the zero lines in (c) are bolded.

nificant over northern Canada (120°W to 60°W) and northern Siberia (90°E to 180°) (Fig. 9c). By contrast, the model oversimulates the storm activity over the continents (0°–120°E and 120°W–60°W) and underestimates the storm activity over the oceans in the midlatitudes (Fig. 9b). The negative anomaly over the oceans and the positive anomaly over the continents are related to the positive moisture fixer scheme. As shown by Fig. 8, the model inputs too much moisture into the continents in the lower troposphere, which in turn increases the latent heat release over these regions and hence intensifies the cyclone activity. On the other hand, in order to conserve the model's total moisture content the specific humidity over the oceans is suppressed by the global moisture correction. The model also fails to simulate the semiannual variation of the storm activity (Fig. 9d), which is a dominant phenomenon over Asia, the North Pacific Ocean, and North America. Further examination of the simulated midlatitude weather systems is needed to identify the causes of these problems, but is beyond the scope of this paper.

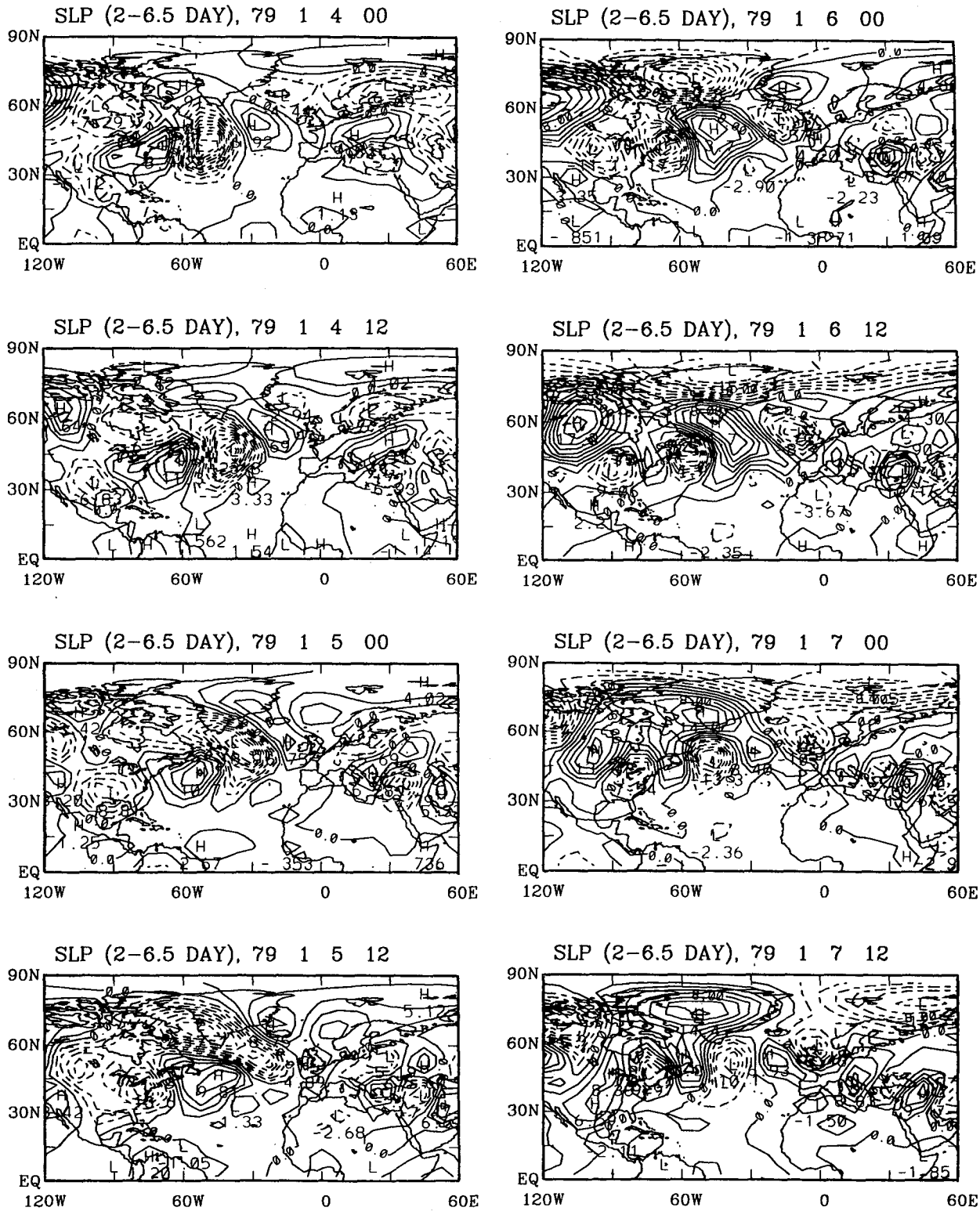

FIG. 6. A case study of simulated cyclone waves (bandpass-filtered SLP) approaching Greenland. The contour interval is 2.0 hPa. The time interval for each panel is 12 h.

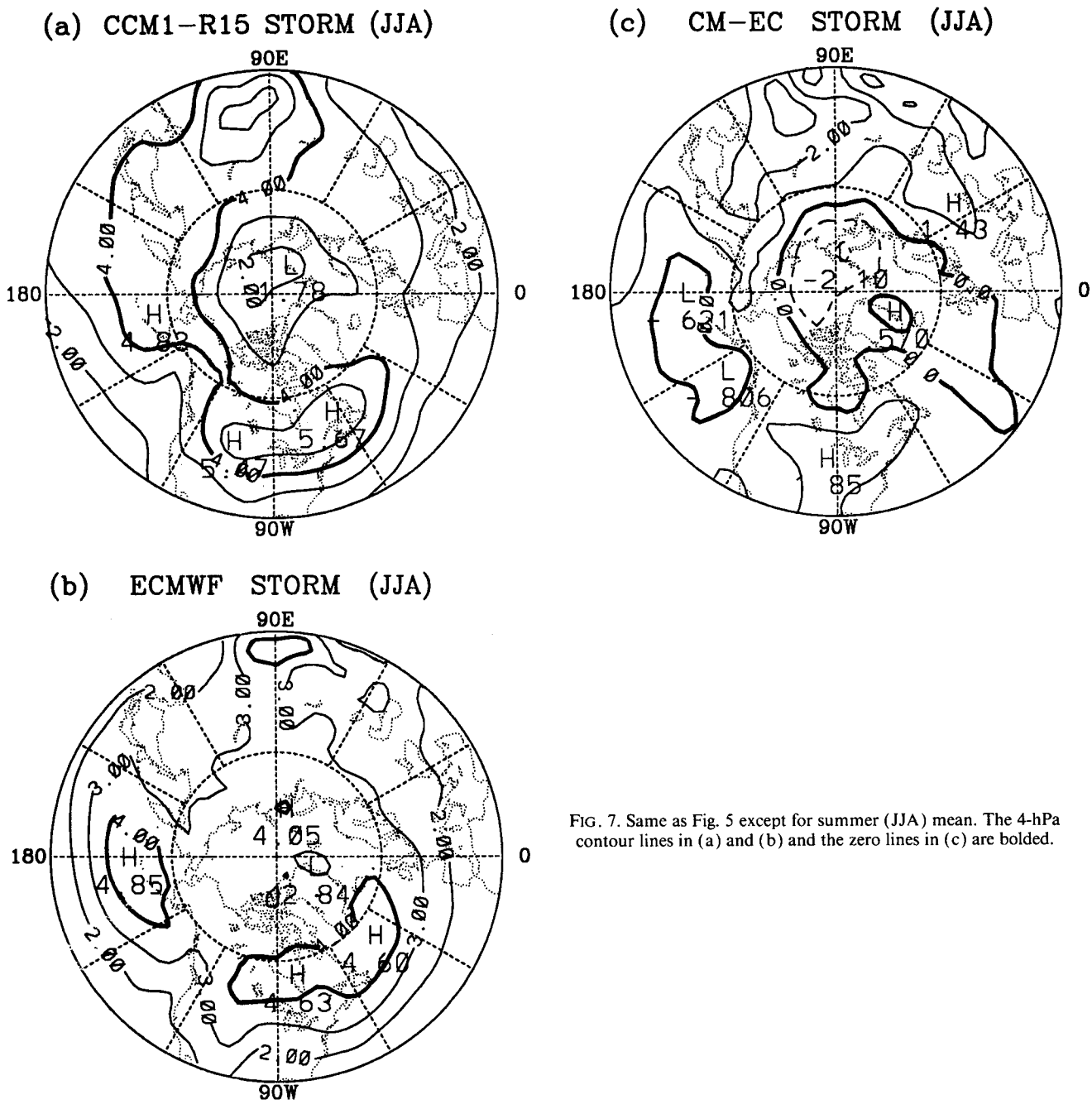

FIG. 7. Same as Fig. 5 except for summer (JJA) mean. The 4-hPa contour lines in (a) and (b) and the zero lines in (c) are bolded.

c. Vertical cross section of height at 70°N

Figure 10 displays the winter mean (DJF) of the vertical cross section of zonally asymmetric height (departure from the zonal mean) along 70°N. The model can simulate the location of troughs and ridges in a broad-scale sense. The model's trough over the west coast of Greenland (60°W), however, does not tilt westward with height in the lower troposphere. The simulated trough over the Beaufort Sea at low levels (north of Alaska, 140°W), by contrast, tilts too far westward with height in the CCM1 because the model does not capture the low-level ridge in this region. This problem is consistent with the bias in this region's storm track. The model overdoes the storm activity over Alaska and northern Canada and, hence, the simulated trough for this region tilts markedly westward with height due to the strong baroclinicity in cyclone waves. By contrast, Fig. 10c shows a positive height bias over the Greenland area (0°–60°W) in the troposphere. From temperature and thickness (500–1000 hPa) analyses (not shown), we found that there is a positive warm bias over this region in spite of the general cold bias throughout the troposphere (Randel and Williamson 1990). These

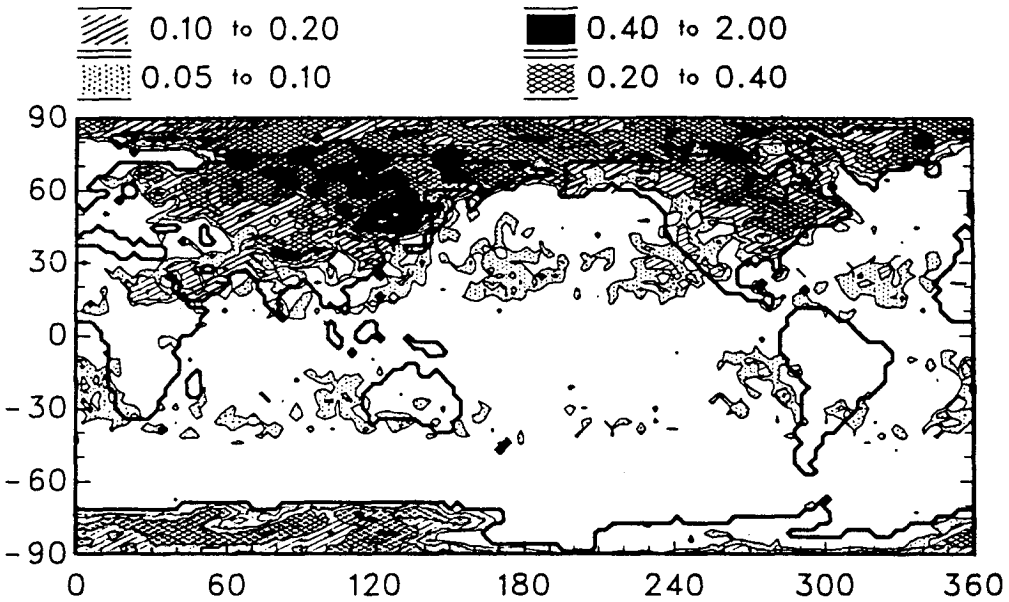

FIG. 8. The winter-average ratio for the lower troposphere between the total (local and global) moisture fixer(s) and the largest of all the other terms in the moisture equation. (After Rasch and Williamson 1990.)

height and warm biases are likely due to the moisture scheme used in the model. The model's averaged annual snowfall accumulation rate is 62.8 cm yr^{-1} over Greenland, which is about twice as large as the observations [33.6 cm yr^{-1}, Bromwich et al. (1993)]. The vertical cross section of model cloudiness along 70°N (not shown) exhibits overcast skies over Greenland. The same problem was also found in the CCM1 simulation of antarctic climate. Tzeng et al. (1993) pointed out that the positive moisture fixer scheme artificially transports too much moisture into Antarctica, which results in overcast skies, too much precipitation, and a warm bias over the continent. Further discussion of the moisture budget of the North Polar Cap is presented in the next section.

From spectral analysis of the winter-mean height field, we found that wavenumber one (Fig. 11) is a baroclinic wave in both model and observations. However, the amplitude of the model's wavenumber one is too large in both middle and upper troposphere (60 m vs 18 m) and too small in the stratosphere (60 m vs 95 m). Although its phase is consistent with the observations in the middle and upper troposphere, its phase is shifted to the west by a quarter wavelength in both the lower troposphere and stratosphere. This phase shift in the model causes the trough axis to tilt westward with height from the north of Hudson Bay (90°W) to the west coast of Alaska (160°W). This analysis (Fig. 11c) confirms the wavenumber one bias pattern in the SLP difference (Fig. 1c) and in the storm track difference (Fig. 5c).

The phase of wavenumber two in CCM1 is the same as that in the observations (not shown). This wave component has an almost barotropic structure (no tilt with height) throughout the troposphere. The location of the two troughs are at Baffin Bay (65°W) and Laptev Sea (125°E) in both model and observations. The simulated amplitude, however, is too small, especially in the upper troposphere (57 m vs 90 m at 300 hPa) and lower stratosphere (85 m vs 130 m at 100 hPa).

d. 500-hPa height

Figure 12 depicts the winter mean (DJF) of the 500-hPa height field. The model in general captures the locations of the major troughs and ridges. The ridge over eastern Greenland, however, is overdeveloped by the model. Like the SLP anomalies (Fig. 1c), the difference between the model and the observations (Fig. 12c) also exhibits a wavenumber one pattern over the Arctic basin. In other words, the simulated cyclonic vortex over the Arctic basin is shifted toward the Bering

FIG. 9. The longitude–time plots for the difference of storm activity between the CCM1 and ECMWF at (a) 70°N, and (b) 45°N. The semiannual variation mode of the difference is presented in (c) for 70°N and (d) for 45°N. The contour interval in (a) and (b) is 0.5 hPa, and 0.25 hPa in (c) and (d). The negative areas are stippled. The vertical lines at 150°E and 30°W in (a), and at 120°E, 120°W, and 60°W in (b) reflect the locations of coasts at that latitude.

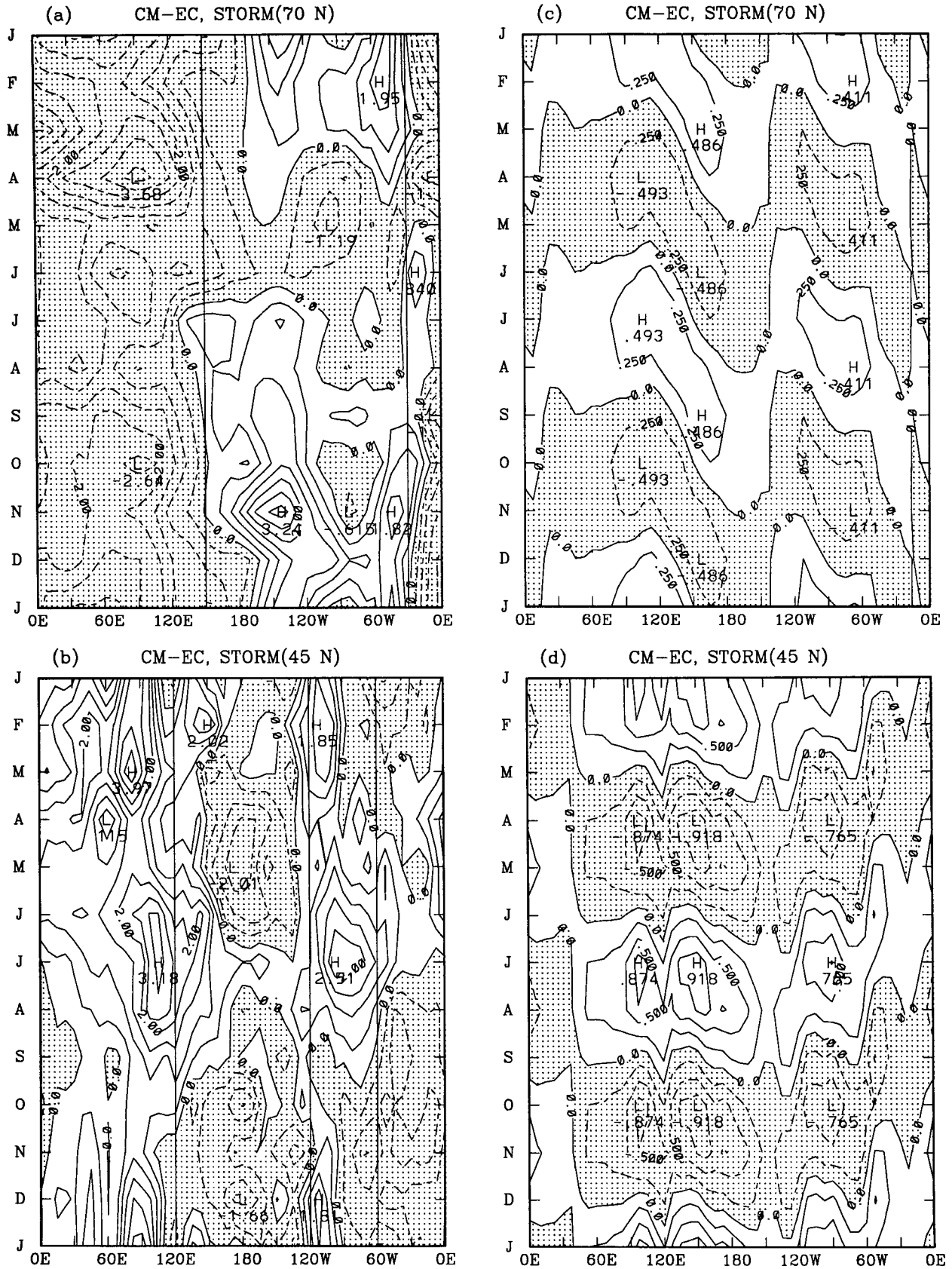
(a) CM–EC, STORM(70 N)
(c) CM–EC, STORM(70 N)
(b) CM–EC, STORM(45 N)
(d) CM–EC, STORM(45 N)
J F M A M J J A S O N D J
0E 60E 120E 180 120W 60W 0E

Strait (180°) instead of being over the center of the Arctic basin as in the observations. This shift causes reduction of the ridge over the west coast of North America and intensification of the ridge over eastern Greenland. Therefore, the simulated North Atlantic storm track is blocked to the west side of Greenland not only by the broadened Greenland topography but also by the intensified ridge over Greenland. This blocking effect leaves a maximum positive anomaly of 500-hPa height over the Barents Sea (40°E) and Norwegian Sea, which is consistent with the SLP analysis (Fig. 1c). Moreover, the southward shift of the ridge over Alaska favors the cyclone waves moving into this region (Fig. 5c).

The 500-hPa height anomalies over the Arctic basin are also attributed to the cyclone activity, that is, less storm activity corresponding to a positive height anomaly. Therefore, the fundamental reasons for these anomalies are related to the model's topography, that is, the broadened Greenland topography and the intensified ridge over Greenland.

The summer (JJA) mean of 500-hPa height is illustrated in Fig. 13. The model output shows a more zonally symmetric pattern (Fig. 13a) than the observations (Fig. 13b). This indicates that the model cannot adequately simulate the summertime planetary-scale waves, especially over northeastern Asia (130°E), the northern Pacific Ocean (180°), and northeastern North America (70°W). The model can capture the trough over the northeastern North America, but the simulated trough is too far south. The southward shift of this trough also forces the storm track to be shifted to the south, as indicated in the section 3b (Fig. 7a). In addition, the model simulates a trough over the northeastern Asia, but there is a ridge in the observations (Fig. 13b). Therefore, the model simulates too much storm activity over this region (Fig. 7c). Moreover, the observed north Pacific trough (180°) is not captured by the model. This bias is consistent with the negative anomaly of storm activity in this region (Fig. 7c).

Spectral analysis of 500-hPa height shows that the model does not correctly simulate the amplitudes and phases of the planetary-scale waves in summer. For example, the amplitudes of wavenumbers two and three are about half of the observations (10 m vs 25 m and 15 m vs 29 m, respectively). Moreover, the phases of simulated wavenumbers one and two are out of phase relative to the observations. Because the stationary planetary-scale waves are generated and maintained by topographic and thermal forcings, these biases in the model are attributed to the model's simulation of these two forcings. The thermal forcing is more important than the topographic forcing in this case because of the prevailing heating source and the weakened zonal winds in this season. In the storm track analyses (Fig. 9), we have pointed out that the errors in the storm simulations are due to 1) the broadened Greenland topography and 2) the positive moisture fixer

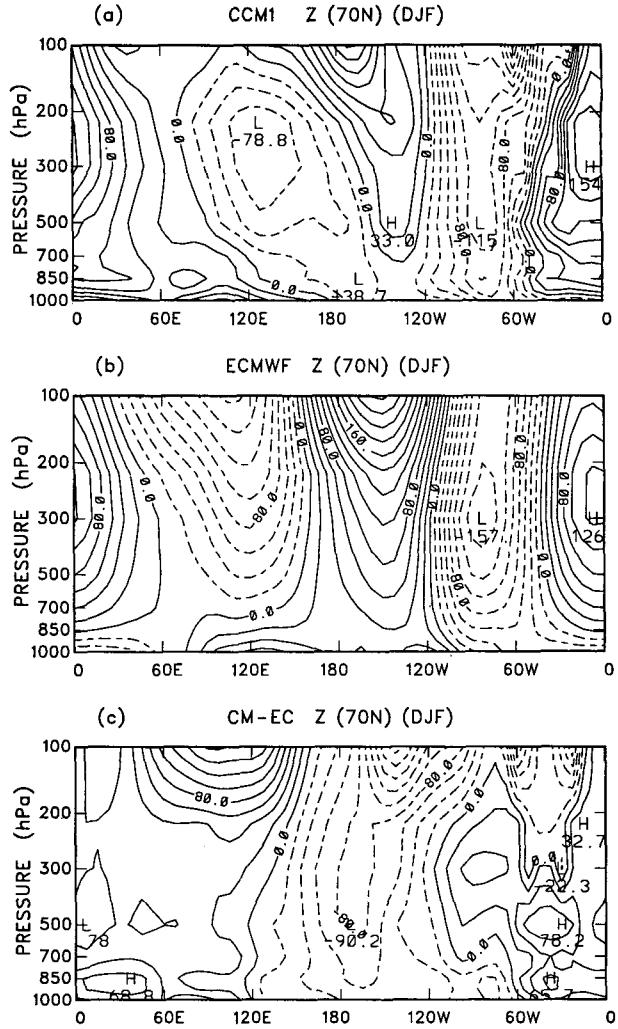

FIG. 10. The vertical cross section of the winter-mean (DJF) zonally asymmetric height field at 70°N for (a) CCM1, (b) ECMWF, and (c) difference between CCM1 and ECMWF. The contour interval is 20.0 m.

scheme, which transports too much moisture into the continents. Therefore, the errors in the simulated planetary-scale waves may also result from these same reasons, particularly the artificial moisture transport, because the errors in the moisture simulation directly impact the latent heat release, the cloud simulation, and hence the energy balance for these regions. In addition, the amplitude of wavenumber five in the model (21 m) is two times larger than the observed (9 m), although their phases are very close to the observed. This bias apparently results from the oversimulated storm activity in the model.

e. Total energy budget

The total energy budget of the atmosphere poleward of 70°N (the North Polar Cap: NPC) can be decom-

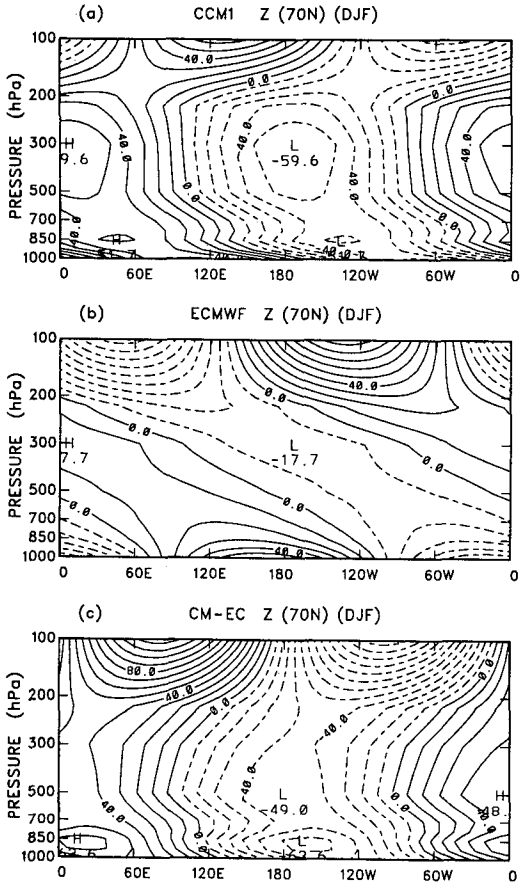

FIG. 11. Same as Fig. 10 except for the wavenumber one component. The contour interval is 10.0 m.

posed into four factors: the rate of change of storage of energy in the atmosphere ($\Delta H/\Delta t$), the net incoming radiation at the top of the atmosphere (F_{top}), the poleward energy flux across hypothetical walls at 70°N (F_{adv}), and the upward energy flux at the earth's surface (F_{sfc}). Therefore, the energy budget equation can be written as [Nakamura and Oort (1988), hereafter referred as NO88]:

$$\Delta\langle H\rangle/\Delta t = F_{\text{top}} + F_{\text{adv}} + F_{\text{sfc}}, \qquad (1)$$

where the vertical and areal average of total energy, $\langle H\rangle$, has the form

$$\langle H\rangle = \frac{1}{A}\int_A\int_0^1 (c_pT + gz + Lq)\frac{P_s}{g}\,d\sigma dA, \quad \text{and}$$

$$F_{\text{adv}} = \frac{1}{A}\int_0^{2\pi}\int_0^1 (c_pT + gz + Lq)V\frac{P_s}{g}\,a\cos 70°\,d\sigma d\lambda,$$

where c_p is the specific heat of dry air at constant pressure, T the temperature, g the acceleration due to the earth's gravity, z the geopotential height, L the latent heat of vaporization, q the specific humidity, P_S the surface pressure, $\sigma = P/P_S$, V the meridional wind, a the radius of the earth, and λ the longitude. The net incoming radiation at the top of the atmosphere is composed of the shortwave solar radiation (F_{SW}) and the outgoing longwave radiation (F_{lw}). The poleward energy flux across 70°N can be broken into two terms: the transient energy flux, TF($\overline{\mathbf{V}'\cdot\nabla H'}$), and the standing flux, SF($\overline{\mathbf{V}}\cdot\nabla\overline{H}$ − TF). For a long-term mean the storage change term ($\Delta H/\Delta t$) approaches zero. Hence, the total energy within the NPC is a balance between the net atmospheric energy transport across the top and bottom ($F_{\text{top}} + F_{\text{sfc}}$) and the net energy flux across the 70°N wall. Table 1 presents the winter (DJF) and summer (JJA) mean of the various energy components for both the CCM1 simulations and NO88's observational results. Although the results from the CCM2 simulation are included in this table, they are discussed in section 3g on model intercomparisons. Note that in order to conserve the total energy the vertical integration used here is over σ coordinate, which is different from the P coordinate used in NO88. Therefore, the transient flux (TF) here is the same as NO88's transient eddy (TE), but the standing flux (SF) here includes all three standing terms in NO88, which are stationary eddy (SE), mean meridional circulation (MMC), and net mass flow (NMF).

In winter, the larger amount of outgoing longwave radiation at the top of the model (168.0 vs 157.7 W m^{-2}) is related to the model's warm bias in the lower to middle troposphere. A similar situation is also found in Antarctica (Tzeng et al. 1993). In summer, the greater outgoing longwave radiation in the model (228.4 vs 209.3 W m^{-2}), however, is due to the simulated cloudiness. The model simulates almost no cloud over the Arctic region during this season. This not only increases the incoming solar radiation to the surface, but also speeds up the ice ablation rates (e.g., Herman and Curry 1984) and hence changes the surface energy budget in the model. However, this difference may also result from the quality of the observational data because of the difficulty of detecting clouds from satellite data (e.g., Rossow 1992). For the net energy flux at the earth's surface, the results from the model are very close to the observations in both winter and summer, even though NO88's results were obtained as the residuals from the energy budget equation.

Both the observations and model simulations show that the TF is the dominant transport term into the North Polar Cap, particularly in summer. The model's TF is larger than the observations, although Randel and Williamson (1990) indicated that the CCM1 can accurately simulate the poleward eddy heat flux. In addition, the CCM1 has a smaller SF than the observed, especially in summer (−1.3 vs 33.7 W m^{-2}), even though Randel and Williamson (1990) indicated that the CCM1's stationary waves are in good overall agreement with the observations. In spite of these biases in the individual energy components the CCM1 can still

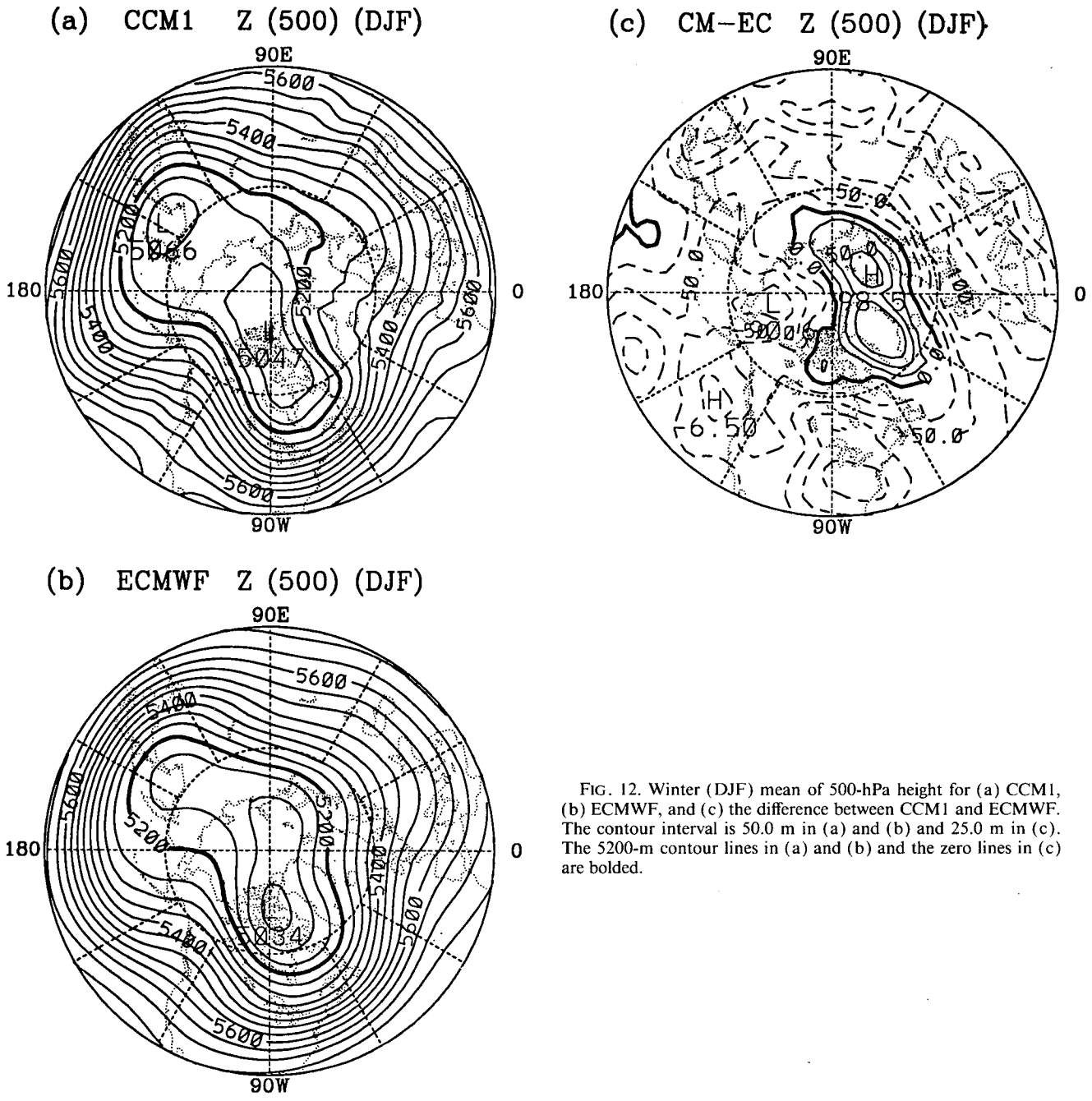

FIG. 12. Winter (DJF) mean of 500-hPa height for (a) CCM1, (b) ECMWF, and (c) the difference between CCM1 and ECMWF. The contour interval is 50.0 m in (a) and (b) and 25.0 m in (c). The 5200-m contour lines in (a) and (b) and the zero lines in (c) are bolded.

balance the total energy in both winter and summer. This is not the case for the CCM2 simulation.

f. Moisture budget

The moisture budget is calculated from the temporally and spatially averaged moisture balance equation (Peixoto and Oort 1983). The equation has the form:

$$\frac{1}{a\cos\varphi}\frac{\partial[\overline{Q_\varphi}]\cos\varphi}{\partial\varphi} = [\bar{E} - \bar{P}], \qquad (2)$$

where φ is the latitude, Q_φ is the vertically integrated moisture transport in the meridional direction, the square brackets denote an areal average, and the overbar a time average.

The mean annual precipitation rate $[P]$ averaged from 70°N to the North Pole is 16.1 cm yr^{-1} in the observations [Peixoto and Oort (1992), hereafter referred as PO92] and 51.9 cm yr^{-1}in the CCM1 (Table 2). The CCM1 has about 3.2 times more precipitation than observed north of 70°N. The simulated evaporation rate ($[E]$) (13.8 cm yr^{-1}) approximates the observed (10.3 cm yr^{-1}, from PO92). However, the

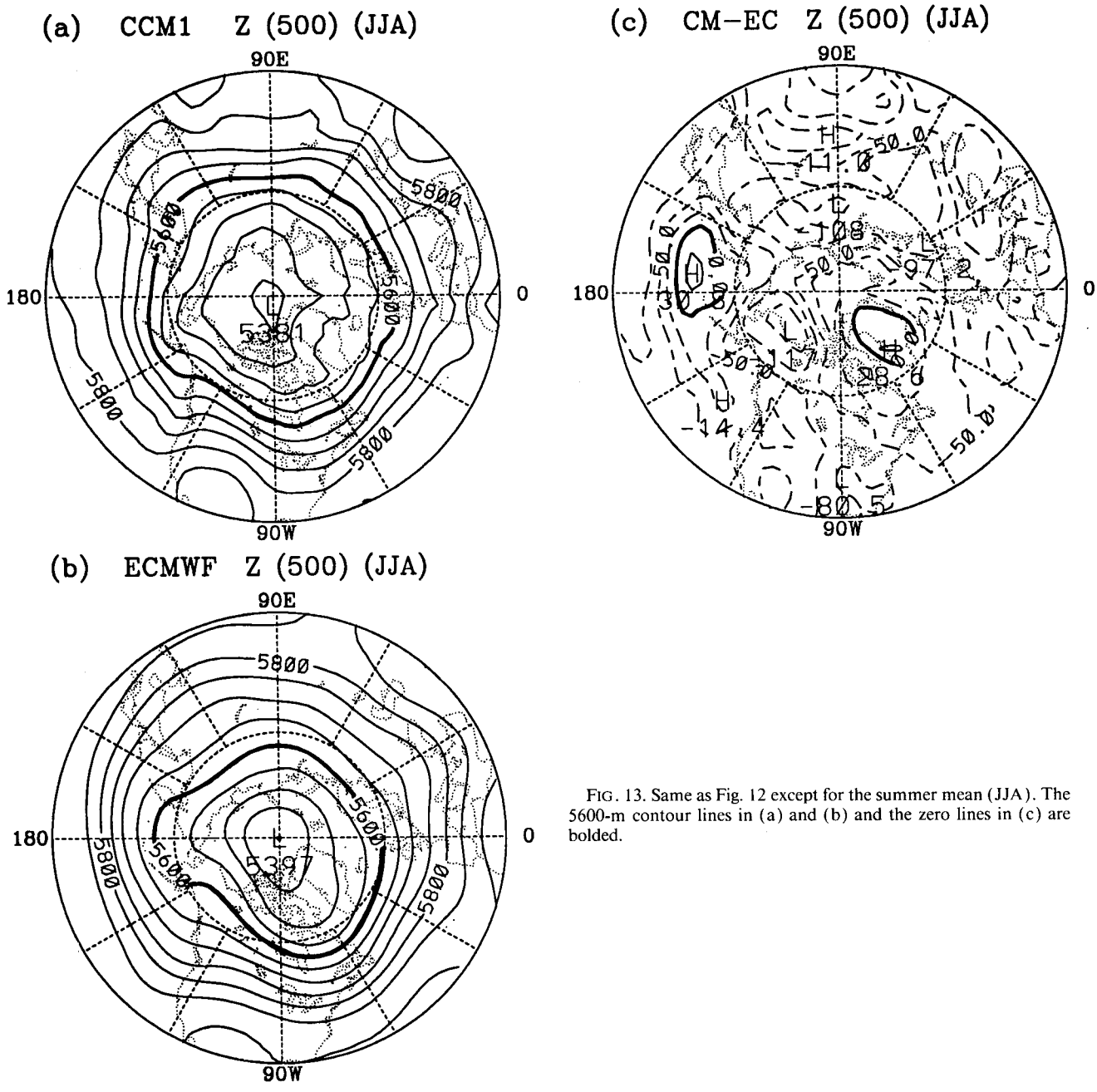

FIG. 13. Same as Fig. 12 except for the summer mean (JJA). The 5600-m contour lines in (a) and (b) and the zero lines in (c) are bolded.

CCM1's net annual precipitation ($[P-E]$) is 6.6 times larger than that of the observations (38.1 cm yr^{-1} in CCM1 vs 5.8 cm yr^{-1} in the observations). In addition, the CCM1 transports 10.5×10^{15} kg yr^{-1} of moisture across 70°N (or 67.8 cm yr^{-1} water equivalent), but the observed (PO92) is only 1.8×10^{15} kg yr^{-1} (or 11.6 cm yr^{-1} water equivalent). About six times more moisture is transported into the North Polar Cap by the CCM1 than is observed.

In addition, the CCM1's annual cycle of precipitable water (W) is consistent with the observations in terms of both amplitude and phase. The annual average of W is 5.4 kg m^{-2} in CCM1 and 6.0 kg m^{-2} in PO92. The maximum of W is in midsummer (July and August) and the minimum is in midwinter (January and February) in both CCM1 and PO92. Therefore, the excessive precipitation rate in CCM1 ($[P]$, 51.9 vs 16.1 cm yr^{-1}) is due to the excessive moisture transported into this region ($[Q]$, 67.8 vs 11.6 cm yr^{-1}). However, the CCM1's moisture flux into the Arctic Basin (67.8 cm yr^{-1}) is much larger than its net annual precipitation ($[P-E]$, 38.1 cm yr^{-1}). Obviously, this excessive moisture (29.7 cm yr^{-1}) must be transported out of this region, which is done in an artificial manner

TABLE 1. Winter (DJF) and summer (JJA) mean of various energy components of the North Polar Cap[a].

	F_{SW}	F_{LW}	F_{top}	TF	SF	F_{adv}	F_{sfc}	Res
				Winter mean				
CCM1	1.9	−168.0	−166.1	69.8	41.5	111.3	41.7	−13.1
CCM2	1.5	−166.0	−164.5	85.8	65.5	151.3	42.2	29.0
NO88[b]	2.	−157.7	−155.7	53.3	51.3	104.6	48.3	−2.8
				Summer mean				
CCM1	220.2	−228.4	−8.2	68.1	−1.3	66.8	−59.2	−0.6
CCM2	210.3	−234.7	−24.4	50.7	11.2	61.9	−55.1	−17.6
NO88	191.7	−209.3	−17.6	50.0	33.7	83.7	−67.3	−1.2

[a] Units are in watts per square meter; F_{SW} is the shortwave radiation into the top of atmosphere, F_{LW} the longwave radiation into the top of atmosphere, F_{top} the net energy flux into the top of atmosphere, TF the transient energy flux across 70°N, SF the standing energy flux across 70°N, F_{adv} the total energy flux across 70°N, F_{sfc} the net energy flux into the atmosphere from the earth's surface, and res the residual of the energy budget equation (res = $F_{top} + F_{adv} + F_{sfc}$).

[b] NO88 represents the data from Nakamura and Oort (1988).

by the positive moisture fixer scheme. In addition, the causes of the excessive simulated poleward moisture transport by the advection term are attributed to both the simulated moisture contents and meridional wind component (v) at 70°N. The bias in the simulated meridional winds is clearly attributable to the SLP simulation, which was discussed in section 3a. The simulated moisture content at 70°N is in error by about 100% because of the positive moisture fixer (Rasch and Williamson 1990). In conclusion, the errors in the moisture budget of the CCM1 are due to the positive moisture fixer scheme and the low horizontal resolution, which distorts the representation of topography in the model and hence the simulated winds. In the observations (PO92), the net annual precipitation [$P - E$], however, does not balance the moisture flux term. The reason for this imbalance (5.8 cm yr^{-1}) is likely to be the uncertainties in the observed precipitation and evaporation rates over the sea ice–covered Arctic Ocean.

Using the semi-Lagrangian transport scheme, the CCM2 definitely can more realistically simulate the various moisture components (Table 2) and the moisture budget equation is now almost balanced; however, the CCM2 simulated net annual precipitation ([$P - E$]) is still about 3.7 times larger than the observed. This comparison indicates that the semi-Lagrangian transport scheme is better than the positive moisture fixer scheme over this region, even though the higher spatial resolution and different physical parameterizations used in the CCM2 also contribute to this improvement. Note that the oversimulation of annual precipitation in the CCM2 is attributable to the errors in the simulated Aleutian low and the northward-shifted storm track in the northern Pacific Ocean, which result in too much moisture transport into this region.

g. A comparison of arctic climate simulated by CCM1-R15, CCM1-T42, and CCM2-T42

The data for the CCM1-T42 analysis are a three-winter mean of once-daily (24-hour interval) data from the NCAR CCM1 seasonal simulation case 244. The CCM2-T42 data are a five-winter (years 11–15) mean of daily averaged data from the NCAR CCM2 20-year control run case 388.

Figure 14a shows that the CCM1-T42 can well capture the location and the pattern of the Icelandic low, although the central pressure is about 10 hPa too low

TABLE 2. Annual values of the areally (70°N–NP) averaged precipitation ([P]) and evaporation ([E]) rates, and of the moisture flux across 70°N ([Q]) from the NCAR CCM1 and CCM2, and the observations.

	[P] (cm yr^{-1})	[E] (cm yr^{-1})	[$P - E$] (cm yr^{-1})	[Q] (cm yr^{-1})	res[a] (cm yr^{-1})	[W] (kg m^{-2})
CCM1	51.9	13.8	38.1	67.8	29.7	5.4
CCM2	37.2	15.5	21.7	17.7	−4.0	6.7
PO92[b]	16.1	10.3	5.8	11.6	5.8	6.0
Ma90[c]				15.8		

[a] Moisture budget error [res] = [Q] − [$P - E$].

[b] PO92: Peixoto and Oort (1992). Climatological average.

[c] Ma90: Masuda (1990). For 1979 annual mean.

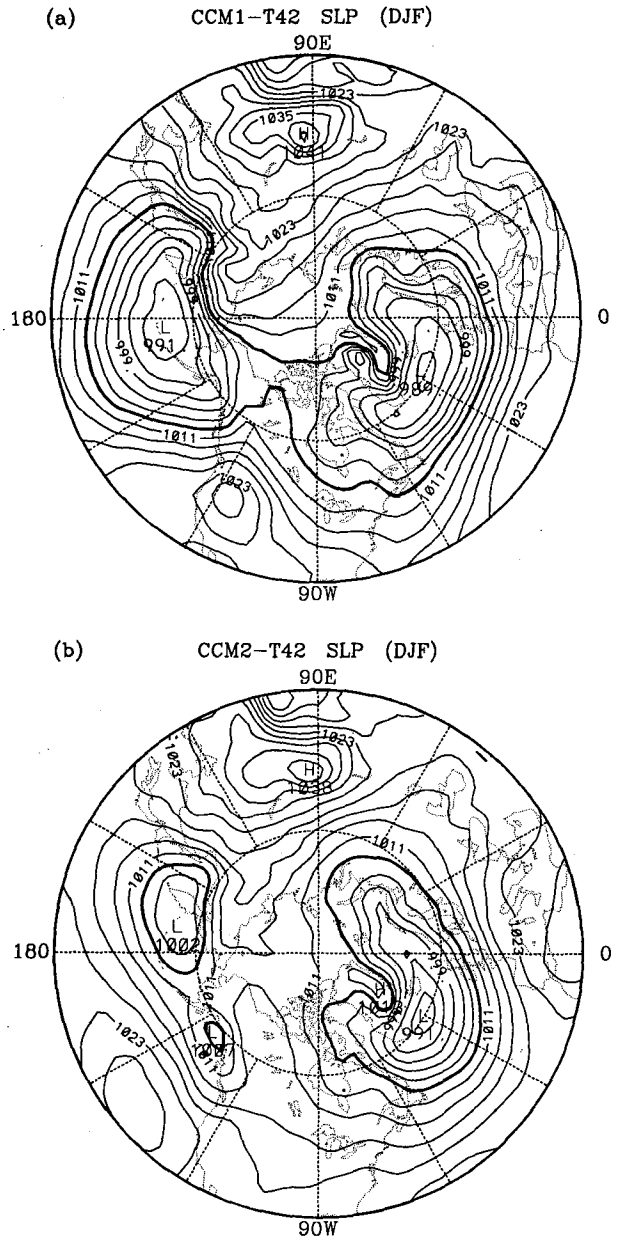

FIG. 14. Winter (DJF) mean of sea level pressure (SLP) for (a) CCM1-T42, and (b) CCM2-T42. The contour interval is 3.0 hPa. The 1008-hPa contour lines are bolded.

and the ridge over Greenland is too strong (cf. Fig. 1). This comparison confirms the argument that the distorted Icelandic low and the distorted North Atlantic storm track are due to the blocking effect of the broadened Greenland topography by the R15 spectral truncation. The increased horizontal resolution also improves the simulation of the Aleutian low and the Siberian anticyclone. However, this does not significantly improve the simulation of the wintertime Beaufort Sea anticyclone nor the annual variation of the arctic stratus clouds (not shown). The CCM1-T42 still simulates more stratus cloud in winter than summer, although the amount of summertime arctic stratus cloud is increased.

The CCM2 at T42 resolution can also well simulate the location and pattern of the Icelandic low, but the intensity of the low center and the ridge over Greenland are still too strong (Fig. 14b). By contrast, the Aleutian low is too weak and too far to the northwest compared to the observations (Fig. 1b). The CCM2 simulates an extra low center over the northwest coast of Canada, which is different from the observations and the CCM1 simulations. This low center intensifies the storm activity over Alaska and western Canada (not shown). This bias of storm activity in the CCM2 is similar to that in the CCM1 simulation (Fig. 5). Also, the CCM2-T42 cannot capture the strong anticyclone over the Beaufort Sea in winter (Battisti et al. 1992), which is important to the transport of sea ice out of the Arctic Ocean, but does simulate a pressure gradient over Farm Strait, which is consistent with the observations (cf. Fig. 1b). In addition, the CCM2 does not balance the total energy over the North Polar Cap (70°N–NP) (Table 1). This is mainly due to the energy flux term. The CCM2 transports too much total energy into the Arctic basin in winter (DJF) but too little in summer (JJA). This indicates that the CCM2 still suffers from errors in the simulated flows.

The CCM2 includes a planetary boundary-layer parameterization and the semi-Lagrangian moisture transport scheme, and the model can now capture more arctic stratus clouds than the CCM1. The annual cycle of low-level cloudiness over the Arctic basin, however, is still out of phase relative to the observations. Moreover, although the CCM2 can better simulate the moisture budget in the Arctic basin than the CCM1 (Table 2), the moisture budget over a larger area has the same magnitude of error as that in the CCM1. The error (residual term) in the moisture budget for the 70°N–NP area is 4 cm yr^{-1} in the CCM2, but jumps to 14.2 cm yr^{-1} for 60°–NP, and to 21.8 cm yr^{-1} for 45°N–NP. These findings confirm Rasch and Williamson's (1990) results that locally the semi-Lagrangian transport scheme has a much smaller error than the positive moisture fixer scheme, but globally the error is approximately the same in both schemes because the semi-Lagrangian transport scheme is nonconservative.

4. Conclusions and remarks

We have investigated the CCM1's simulation of modern arctic climate by comparing the history data from a 5-year seasonal cycle simulation to the ECMWF global analyses and to the CCM2 simulations. The sea-level pressure, storm activity, vertical cross section of height, 500-hPa height, total energy budget, and moisture budget are analyzed to identify the biases in the

model. The results show that there is a negative SLP anomaly, too much storm activity, and hence anomalously strong baroclinicity to the west of Greenland and vice versa to the east of Greenland. This is mainly due to the blocking effect of Greenland. The broadened Greenland topography blocks the climatological path of the North Atlantic storm track. Moreover, the oversimulated ridge over Greenland not only intensifies the blocking effect of Greenland, but also steers the cyclone waves clockwise around Greenland. The blocking effect cuts off the migration of cyclone waves into the Norwegian Sea and finally into the Barents Sea. Therefore, it results in a positive SLP and height bias to the east of Greenland and a negative SLP and height bias to the west.

During summer (JJA), the model cannot correctly simulate the major axis of the subtropical anticyclone over the Pacific Ocean. In addition, the model incorrectly simulates the planetary-scale waves and oversimulates the synoptic-scale waves (the storm activity) over the midlatitude continents. These errors result from model's positive moisture fixer scheme, which artificially transports too much moisture into the continents. The excessive moisture input changes the cloud simulation, provides extra diabatic (latent) heat to the planetary-scale waves, and supplies energy and moisture to the cyclone waves. On the other hand, the model fails to simulate the prevailing low-level stratus clouds over the Arctic basin during summer. This is due to the errors in the simulated SLP and the negative bias of storm activity over this region, which suppress the moisture transport into this region in summer. Our analysis shows that this bias mainly results from the low horizontal resolution in the model (R15), although the absence of a planetary boundary-layer parameterization (Randall et al. 1985) and the prescribed constant thickness of sea ice (Battisti et al. 1992) also contribute to this error.

The energy budget analysis shows that the model's total energy is conserved inside the North Polar Cap (70°N–NP). The individual energy components are, however, not consistent with the observations. Both the incoming solar radiation and outgoing longwave radiation across the top of the model atmosphere are too large in the model because of the errors in the simulated temperature and cloudiness for this area. The energy transported by the transient flux (TF) across 70°N is also too large in the model. This is likely due to the positive moisture fixer scheme, which transports too much moisture and hence latent heat into this region. By contrast, the energy transported into the Arctic basin by the standing flux (SF) is too small in the model, especially during summer. This error is attributed to the simulated planetary-scale waves. The error in the planetary-scale waves is mainly due to the diabatic heating in the model, which again results from the moisture-fixer scheme.

The precipitation rate, the net precipitation rate, and the moisture flux across 70°N are too large in the model. These errors are not only due to the positive moisture fixer scheme but also due to the simulated meridional wind component (v), because the model fails to adequately simulate both the planetary-scale and synoptic-scale waves. Nevertheless, the model's precipitable water over the North Polar Cap approximates the observations. This indicates that the excessive moisture has to be immediately precipitated out from the model atmosphere or transported out of this region artificially by the positive moisture fixer. In conclusion, the biases in the atmospheric moisture budget in the model are due to the errors in the moisture fixer scheme and the simulated meridional winds, while the imbalance in the observations result from the quality of the precipitation and evaporation data over the Arctic basin.

Finally, it is clear that the CCM1 at R15 resolution is not adequate for climate change studies over high northern latitudes, especially when the response of the climate system is strong over this region, for example during the Little Ice Age and the last glacial period. Higher horizontal resolution (e.g., T42) may remedy the errors due to the topographic distortion in the CCM1-R15. The positive moisture fixer scheme urgently needs to be changed. The semi-Lagrangian transport scheme, on the other hand, may locally relieve the errors in the moisture simulation, but its global error is as serious as the positive moisture fixer scheme.

Acknowledgments. This work was supported in part by NASA Grant NAGW-2718 to DHB, NOAA Grant NA90AA-D-AC504 to DHB, an internal grant of The Ohio State University to RYT, and NASA Grant NAGW-2666 to TRP. The CCM1 simulations were performed on the Cray Y-MP of the Ohio Supercomputer Center, which is supported by the State of Ohio. The ECMWF data were unpacked on the Cray Y-MP of NCAR, which is sponsored by the National Science Foundation. The computational (CPU) time on the NCAR Cray Y-MP was provided by Cray Research Inc.

REFERENCES

Battisti, D. S., D. L. Williamson, and R. E. Moritz, 1992: Simulation of the Arctic climatology with the NCAR CCM2. Preprints, *Third Conf. Polar Meteorology and Oceanography,* Portland, OR, Amer. Meteor. Soc., 130–136.

Broecker, W. S., D. M. Peteet, and D. Rind, 1985: Does the ocean–atmosphere system have more than one stable mode of operation? *Nature,* **315,** 21–26.

Bromwich, D. H., F. M. Robasky, R. A. Keen, and J. F. Bolzan, 1993: Modeled variations of precipitation over the Greenland Ice Sheet. *J. Climate,* **6,** 1253–1268.

Hansen, J., G. Russell, D. Rind, P. Stone, A. Lacis, S. Lebedeff, R. Ruedy, and L. Travis, 1983: Efficient three-dimensional global models for climate studies: Model I and II. *Mon. Wea. Rev.,* **111,** 609–662.

Held, I., 1993: Large-scale dynamics and global warming. *Bull. Amer. Meteor. Soc.,* **74,** 228–241.

Herman, G. F. and R. Goody, 1976: Formation and persistence of summertime arctic stratus clouds. *J. Atmos. Sci.*, **33,** 1537–1553.

——, and J. A. Curry, 1984: Observational and theoretical studies of solar radiation in arctic stratus clouds. *J. Climate Appl. Meteor.*, **23,** 5–24.

Masuda, K., 1990: Atmospheric heat and water budgets of polar regions: Analysis of FGGE data. *Proc. NIPR Symp. Polar Meteorology Glaciology,* Vol. 3, 79–88. [Available from the National Institute of Polar Research, 9-10, Kaga 1-chome, Itabashi-ku, Tokyo 173, Japan.]

Nakamura, N., and A. H. Oort, 1988: Atmospheric heat budgets of the polar regions. *J. Geophys. Res.*, **93,** 9510–9524.

Peixoto, J. P., and A. H. Oort, 1983: The atmospheric branch of the hydrological cycle and climate. *Variations in the Global Water Budget,* A. Street-Perrott, M. Beran, and R. Ratcliffe, Eds., D. Reidel, 5–65.

——, and ——, 1992: Water cycle. *Physics of Climate,* American Institute of Physics, 270–307.

Ramanathan, V., E. J. Pitcher, R. C. Malone, and M. L. Blackmon, 1983: The response of a spectral general circulation model to refinements in radiative processes. *J. Atmos. Sci.*, **40,** 605–630.

Randall, D. A., J. A. Abeles, and T. G. Corsetti, 1985: Seasonal simulations of the planetary boundary layer and boundary-layer stratocumulus clouds with a general circulation model. *J. Atmos. Sci.*, **42,** 641–676.

Randel, W. J., and D. L. Williamson, 1990: A comparison of the climate simulated by the NCAR Community Climate Model (CCM1:R15) with ECMWF analyses. *J. Climate,* **3,** 608–633.

Rasch, P. J., and D. L. Williamson, 1990: Computational aspects of moisture transport in global models of the atmosphere. *Quart. J. Roy. Meteor. Soc.*, **116,** 1071–1090.

Rintoul, S. R., 1992: Report: Ocean–atmospheric linkages. *Modeling the Earth System.* D. Ojima, Ed., UCAR/Office for Interdisciplinary Earth Studies, 165–180.

Rossow, W. B., 1992: Some results from ISCCP and other cloud climatologies. Preprints, *Third Conf Polar Meteorology and Oceanography,* Portland, OR, Amer. Meteor. Soc., Boston, 1–3.

Stanton, B. R., 1991: Ocean circulation and ocean–atmosphere exchange. *Clim. Change,* **18,** 175–194.

Trenberth, K. E., and J. G. Olson, 1988: ECMWF global analyses 1979–1986: Circulation statistics and data evaluation. NCAR Tech. Note, NCAR/TN-300+STR, National Center for Atmospheric Research, 94 pp. [Available from National Center for Atmospheric Research, P.O. Box 3000, Boulder, CO 80307.]

Tsay, S.-C., and K. Jayaweera, 1984: Physical characteristics of Arctic stratus clouds. *J. Climate Appl. Meteor.*, **23,** 584–596.

Tzeng, R.-Y., D. H. Bromwich, and T. R. Parish, 1993: Present-day Antarctic climatology of the NCAR Community Climate Model Version 1. *J. Climate,* **6,** 205–226.

Vowinckel, E., and S. Orvig, 1970: The climate of the North Polar Basin. *World Survey of Climatology.* Vol. 14, *Climates of the Polar Regions,* S. Orvig, Ed., Elsevier, 129–252.

Walsh, J. E., and R. G. Crane, 1992: A comparison of GCM simulations of Arctic climate. *Geophys. Res. Lett.*, **19,** 29–32.

Washington, W. M., and G. A. Meehl, 1989: Climate sensitivity due to increased CO_2: Experiments with a coupled atmosphere and ocean general circulation model. *Climate Dyn.*, **4,** 1–38.

Williamson, D. L., 1990: CCM progress report—July 1990. NCAR Tech. Note, NCAR/TN-351+PPR, National Center for Atmospheric Research, 109 pp. [Available from National Center for Atmospheric Research, P.O. Box 3000, Boulder, CO 80307.]

——, J. T. Kiehl, V. Ramanathan, R. E. Dickinson, and J. J. Hack, 1987: Description of NCAR Community Climate Model (CCM1). NCAR Tech. Note, NCAR/TN-285+STR, National Center for Atmospheric Research, 112 pp. [Available from National Center for Atmospheric Research, P.O. Box 3000, Boulder, CO 80307.]